# Effect of Internal and External Swirls on Near-Field Spray Characteristics of Swirl Burst Injectors Using High-Speed X-Ray Imaging

Md Shakil Ahmed<sup>1</sup>, John Cary<sup>2</sup>, Kamel Fezzaa<sup>3</sup>, Samuel Clark<sup>4</sup>, Steve McClain<sup>5</sup> and Lulin Jiang<sup>6</sup>\*

<sup>1,2,5,6</sup>Department of Mechanical Engineering, Baylor University, Waco, TX 76798, USA <sup>3,4</sup>X-Ray Imaging Group, Advanced Photon Source, Argonne National Lab, Argonne, IL 60439, USA

The present study investigates the effect of internal and external swirls on water spray characteristics at the near field of the exit of a novel Swirl Burst (SB) twin-fluid injector. Clean and efficient liquid-fuel combustion highly depends on atomization performance. Compared to conventional injectors discharging a jet core/sheet, the SB atomizers generate fine sprays immediately via primary atomization by bubble-bursting and secondary atomization by shear layer instabilities. A previous design integrated swirling atomizing flows and successfully enhanced secondary atomization. This design resulted in clean, compact lean-premixed combustion of distinct fuels, potentially enabling small-core fuel-flexible combustors. In the current work, internal and/or external swirls are added to enhance either the primary atomization (SBP), the secondary atomization (SBS), or both simultaneously (SBC and SBCR with reverse swirls). The near-field atomization mechanism and spray characteristics of the different SB injector designs are investigated using high-speed (5 Mfps) x-ray imaging with an Air to Liquid Mass Ratio (ALR) of 1.75 while comparing key injector geometrical parameters. Results show that all injectors produce fine droplets, with over 95% under 18 µm in size, at the injector immediate exit. The SBCR injector exhibits the most uniform droplet size distribution and improved stability. SBP produces the widest sprays, while SBS has the narrowest. Overall, while all the SB injectors achieve fine atomization, the SBCR injector offers the best spray uniformity and stability, and a larger spray angle than the SBS.

<sup>&</sup>lt;sup>1</sup> Graduate Research Assistant, Department of Mechanical Engineering, Baylor University

<sup>&</sup>lt;sup>2</sup> Undergraduate Research Assistant, Department of Mechanical Engineering, Baylor University

<sup>&</sup>lt;sup>3</sup> Supporting Author, Physicist at Argonne National Laboratory

<sup>&</sup>lt;sup>4</sup> Supporting Author, Advanced Photon Source Scientist at Argonne National Laboratory

<sup>&</sup>lt;sup>5</sup> Professor, Department of Mechanical Engineering, Baylor University, and AIAA Senior Member

<sup>&</sup>lt;sup>6</sup> Assistant Professor, Department of Mechanical Engineering, Baylor University, and AIAA Senior Member \*Corresponding Author Email: Lulin Jiang@baylor.edu

#### Nomenclature

ALR = Air-to-Liquid Mass Ratio

D = inner diameter of liquid tube and injector exit orifice

D<sub>t</sub> = outer diameter of grooved surface Dh = inner diameter of grooved surface

 $\alpha$  = angle of swirl imparted to the atomizing air at the liquid tube tip

H = gap height between liquid tube and exit orifice

AB = Air Blast PS = Pressure-Swirl FB = Flow Blurring AA = atomizing air SB = Swirl Burst

ISN = Injector Swirl Number SBP = Swirl Burst Primary SBS = Swirl Burst Secondary SBC = Swirl Burst Combined

SBCR = Swirl Burst Combined Reverse

SMD = Sauter Mean Diameter FFT = Fast Fourier Transformation

#### I. Introduction

The quest for clean, renewable energy sources is a driving factor in the current social climate. Due to the polluting factor and future scarcity of typical fossil fuels, other non-traditional forms of fuels are being explored to achieve clean and complete combustion. One sustainable alternative is biodiesel, which is produced from vegetable oils or animal fats [1]. However, the cost of producing biodiesel using today's technology is an expensive and timeconsuming process, causing a demand for cost-effective and readily available alternative fuels. Yet, these alternatives have fuel properties, such as their increased viscosity compared to conventional fossil fuels, which hinder their use in conventional injectors that are highly sensitive to fuel property variation, limiting combustion performance [2]. As a result, any attempts to atomize these alternative fuels using conventional injection, such as air blast (AB) and pressure swirl (PS) injectors, have had limited success, creating a need for different injector technology to fully atomize more viscous fuels. On the other hand, "drop-in" renewable fuels with the similar properties compared to diesel, such as renewable diesel and renewable jet fuels, are explored to enable clean combustion without modifying existing engines. However, the conventional injectors generate sprays by jet breaking mechanism, which still yield ligaments and large droplets. Those non-fully vaporized large liquid parts enter combustion zone and lead to incomplete combustion emitting soot, unburned hydrocarbons, carbon monoxide (CO) and nitrogen oxides (NOx) regardless of the conventional fossil fuels or biofuels. Furthermore, fuel viscosity significantly increases during the more-frequently occurred cold days due to the changing climate. Hence, fuel injectors that can transform the jet/sheet-based atomization and encompass high viscosity tolerance are indispensable to enable complete and clean combustion of various liquid fuels for high energy resilience.

One such technology is the flow-blurring (FB) injector. The conventional AB injector simply uses pressurized air to force liquid from the injector nozzle, creating a jet stream of large liquid droplets and only viable with low-viscosity fuels. Unlike the traditional AB injection, the FB injector design utilizes rapid internal two-phase mixing and the pressure difference at injector exit to create fine atomization due to bubble-bursting, which is called *the primary atomization*. Secondary atomization occurs through two-phase interactions via shear layer instabilities of the liquid parts and the surrounding gas at the distinct velocities and densities [3–5]. It has been shown by Gañán-Calvo [6], Jiang et al.[1–3, 7], Simmons and Agrawal [1–3, 7, 8] and Qavi et al. [4] to outperform AB injection because of its lower injection pressure, immediate droplet evolution, smaller droplet size, and shorter atomization length, even with highly viscous fuels. Figures 1(a) and 1(b) visually illustrate the near-field liquid jet and sprays respectively from AB and FB injectors.

FB injection resulted in relatively larger droplets at the spray periphery and yielded ligaments, though thin ones, for highly viscous liquid (such as glycerol) [2, 3]. In order to further enhance the atomization, the group developed the swirl burst (SB) concept, which introduced swirl grooves on its exit and integrated the FB injector geometries to

direct swirling atomizing air (AA) more robustly mixing with the liquid phase externally [9, 10]. The SB design enhanced the secondary atomization, which is further defined as SBS. Compared to FB injection, the SBS has successfully halved the atomization completion length [9, 10] and produced a finer spray with a wider spray cone as visualized by the near field liquid spray shown in Figure 1(c). Thus, it resulted in more compact, less-lifted flames and greater combustion efficiency with ultra-low emissions of NOx and other pollutants, even for viscous oils such as straight vegetable oil [11, 12].

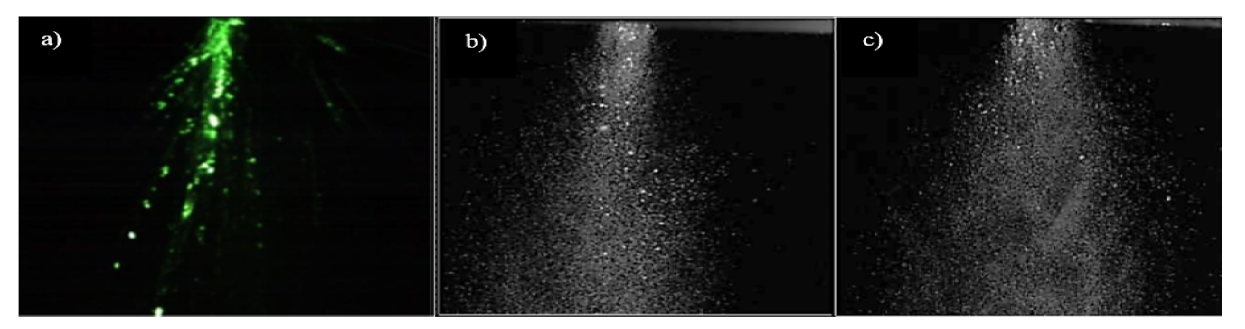


Fig. 1 Injector near field spray images for (a) AB [3], (b) FB, and (c) SBS injectors [9, 10].

In order to determine the optimal swirl-burst (SB) design, the group then developed multiple other iterations of the SB design, incorporating its geometry onto different parts of the injector nozzle and exit and combining swirl placements. The first iteration is the swirl-burst-primary (SBP) injector, which only features swirled grooves on the liquid tube exit to improve primary atomization; the second is the swirl-burst-combined (SBC) injector, which combines both SBP and SBS injector designs to feature swirled grooves on both inner and outer pieces; and the third is the swirl-burst-combined-reverse (SBCR) injector, which features a reverse swirled orientation on the chamfered injector exit compared to the liquid tip swirls so that the two grooves rotate in opposite directions. By quantitatively investigating the resulted spray characteristics for each injector using a high-speed x-ray imaging system, the four SB injectors were tested and determined by which one has the greatest spray atomization properties.

### II. Objectives

Motivated by the preliminary success of the SBS injector, the current study will investigate the water spray features in the near field of the SBS, SBP, SBC, and SBCR injectors to understand the effect of the injector swirl placement. In order to accurately compare each design, the other key geometry, such as the opening angle, liquid tube inner diameter, height between liquid tube nozzle and injector exit hole, and Injector Swirl Number (ISN), remain the same values for each iteration of injector.

### III. Experimental Setup

Figure 2(i) shows the SBS design with the swirl on the outer piece of the injector, i.e. the chamfered opening. Since the swirled grooves are only present on the exit orifice for the SBS design, the inner injector piece that is used only creates primary atomization consistent with FB injection without introducing a radial element of air entry into the internal liquid tube compared to the SBP injector in Fig. 2(ii). However, after the droplets and ligaments, if there are, leave the injector, the secondary atomization then further atomizes the spray due to Rayleigh-Taylor instabilities between the AA in the near field and the liquid phase [10], reintroducing the radial element of shear layer instability that the FB and SBP lacks. Figure 2(ii) illustrates the SBP design and working principle. Like the FB injector [1], the SBP injector features the same principle of primary atomization by internal bubbling and bubble bursting, but also combines swirled grooves on the tip of the internal injector piece to incorporate a radial element of AA into the liquid stream from the injector nozzle. The SBP injector works by a set of geometric conditions: that the liquid tube diameter (D) to gap region (H) ratio is 4:1 or bigger, causing the inner piece to be suspended inside of the injector frame. Once the AA is directed through the swirled grooves, it gains a tangential velocity vector in relation to the liquid nozzle, creating a vortex that enhances the bifurcation process and increases fine atomization. Once at the injector exit, the pressure of the air-liquid mixture drops and creates shear layer instabilities due to the different velocity vectors of the air and air-liquid mixture. In order to control the curvature of the swirl, the Injector Swirl Number (ISN) was developed from the guiding design parameters by previous researchers [13]. The ISN is defined by Eq. (1):

ISN = 
$$\frac{2}{3} \times \frac{1 - (dh/d_t)^3}{1 - (dh/d_t)^2} \times \tan(\alpha)$$
 (1)

where,  $d_t$  is the tip diameter of the grooves,  $d_h$  is the hub diameter, which is approximately equal to the exit orifice diameter, and  $\alpha$  is the exit angle of the swirl grooves, which is defined as the angle between the tangent line to the exit of the groove at the inner wall relative to the axis of spray. This angle is approximately the angle at which the air travels as it leaves the groove [14]. All iterations of the SB injectors share key geometry in order to minimize data error from other uncontrolled characteristics. The key geometry used is a D of 1.5 mm, an H of 0.375 mm, an injector opening angle of 120 degrees, an  $\alpha$  of 71.6 degrees, and the ISN equaling to 2.6.

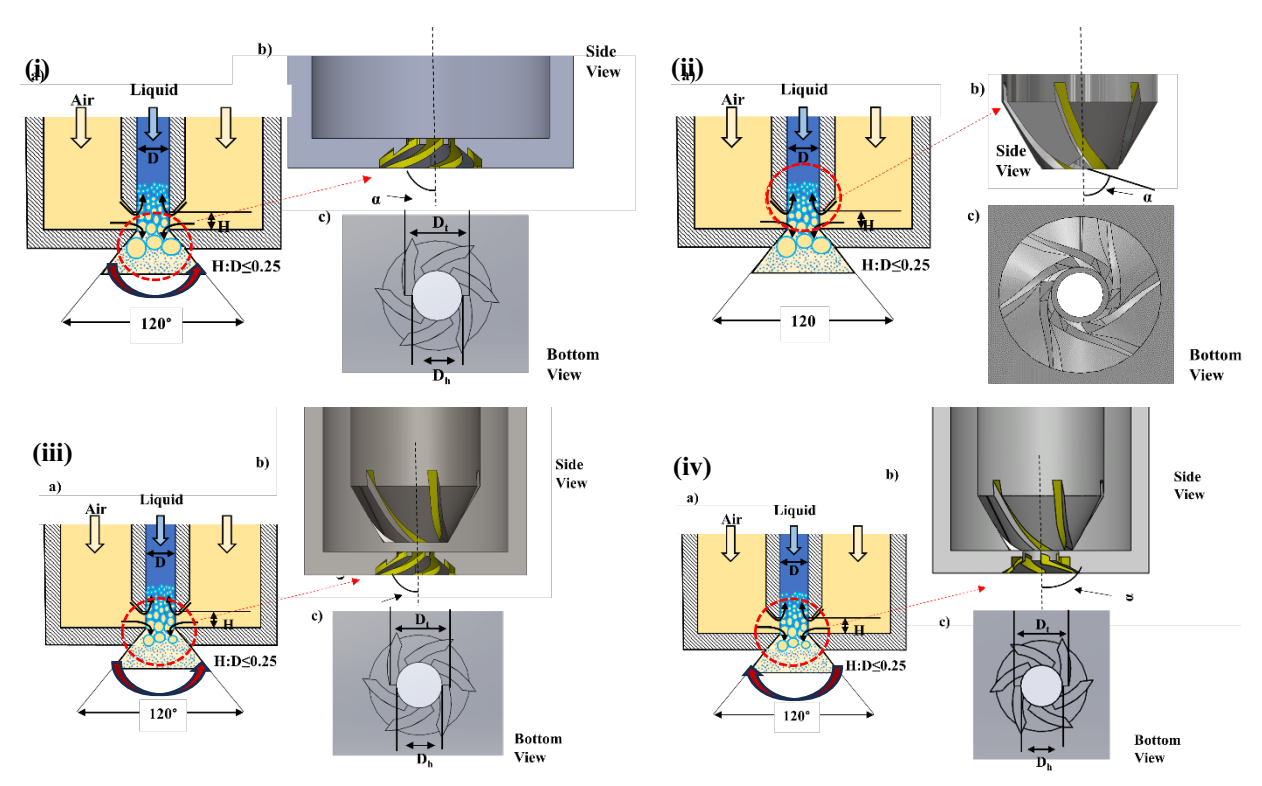


Fig. 2 Different injector designs (i) SBS, (ii) SBP, (iii) SBC and (iv) SBCR injectors [ (a): bubble bursting atomizing visualization and (b, c): visual and important parameters].

Figure 2(iii) shows the SBC injector, which is combination of the SBP and SBS injector designs. Since it incorporates the swirl grooves into both the inner and outer pieces, the SBC features both enhanced primary and secondary atomization compared to FB injection. The SBC injector prioritizes sharing the ISN from the primary and secondary swirls, as well as the same D:H ratio, in order to remain consistent with SBP and SBS key geometry. Additionally, the swirls on the SBC injector share the same direction of rotation in order to increase the vorticity factor of the swirled AA. Figure 2(iv) illustrates the SBCR injector, which shares identical key geometry with the SBC injector but with the external and internal swirls oriented in a reversed direction.

Figure 3 shows a schematic of the experimental setup. The experiment will be run using a high-resolution x-ray technique to take images of the spray in the near field. To initiate spray, compressed air is passed through filters and a water trap before arriving at the injector setup. The conditioned AA is supplied to the injector and controlled with an Alicat Mass Flow Controller (Model MCR-250SLPM-D) with an accuracy of  $\pm 0.8\%$  of the reading  $\pm 0.2\%$  of the full scale of 250 SLPM. The air will then be supplied through a  $\frac{1}{4}$ " ID tube with an operating temperature range of  $\pm 0.40\%$  F and a maximum pressure of 180 psi and then a  $\frac{1}{4}$ " ID welded steel tube with an operating temperature range from  $\pm 0.60\%$  F and maximum pressure of 3,700 psi @ 72% F. The pressure for the AA is monitored by a PX409-100GUSBH series pressure transducer with a pressure range of 0 to 100 gpsi with an accuracy of  $\pm 0.08\%$  BSL. The liquid is supplied by a Cole-Parmer Digital Peristaltic Pump (Masterflex L/S Model 07522-30) with a  $\pm 0.1\%$  F.S.

and in-house built pulsation dampener. The liquid is then delivered through a ½" OD rubber hose with an operating temperature range of 25° to 150° F and maximum pressure of 350 psi @ 72° F and then a ¼" OD welded steel tube with an operating temperature range from -65° to 800° F and maximum pressure of 3,700 psi @ 72°. The liquid pressure is also monitored by a PX409-100GUSBH series pressure transducer with a pressure range of 0 to 100 gpsi with an accuracy of ±0.08% BSL. The injector is housed inside of a spray chamber, 14"x14"x14" acrylic cube with an aluminum funnel base, to minimize excess spray contamination, and features polyimide (Kapton) film to absorb x-ray absorption during the imaging process. The spray chamber also features ports for surrounding inert air in order to keep the polyimide film from fogging during the spray experiment. The effect of varying placement of the SB swirl geometry in relation to a fixed ALR on the spray characteristics. will be quantitatively investigated. The experiments were operated with a liquid flow rate of 12 mL/min, an air flow rate of 17.46 standard liters per minute (SLPM), resulting in the ALR of 1.75.

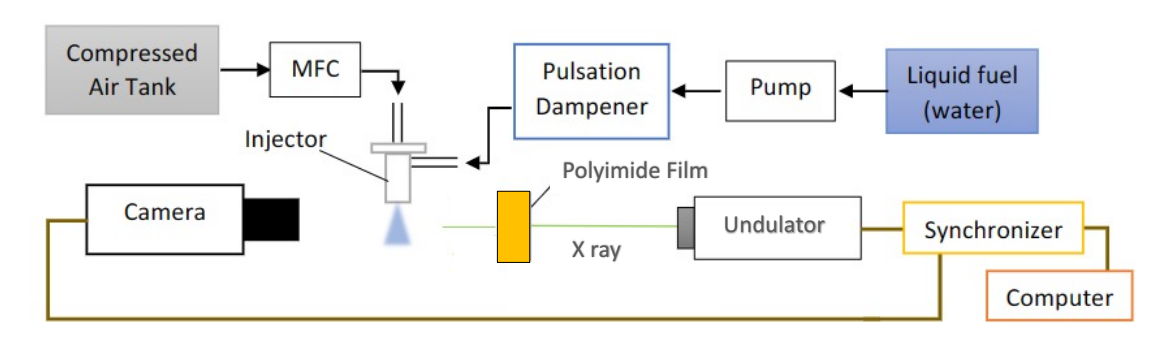


Fig. 3 Experimental setup diagram of the high-speed x-ray imaging [15]

The high-speed X-ray imaging at the Argonne National Lab utilizes a Shimadzu HPV-X2 camera (Serial No 1778057L0122), with a temporal resolution of 5 million frames per second (fps) for external spray imaging at the camera exposure of 110 ns, and a spatial resolution of 3µm per pixel with the field of view (FOV) of 1.2mm (radial) x 0.75 mm (axial) in the near field of each injector exit. X-ray exposure time is 100 ps, i.e., the X-ray pulse duration. The speed of X-ray is 6.5 MHz (153 ns time interval between 2 pulses). The X-ray is not like laser that only illuminate during the pulse. The X-ray will decay along time after each pulse (not like laser immediately gone), which means sometimes the camera exposure (~110 ns) might not be there during the X-ray pulse (100 ps). When this happens, it will still generate X-ray images, which are however darker than those captured when the X-ray pulse falls into the camera exposure. The near field of the injector exit is mapped and moving the FOVs in horizontal (i.e., radial) and vertical (i.e., axial) directions using a traversing-system controlled optical table where the spray chamber is set up. Two sets of consecutive 128 photos per record were captured at each location (i.e., each FOV). The undulator provides 5Mhz imaging with a period of 3.3 cm at a gap of 15mm. The short pulse duration allows the small, fast-moving droplets perfectly frozen in the captured images.

As shown in the Fig. 4, the process of getting processed image from the raw image was completed using different macros and ImageJ software plug-ins. The raw images were first processed with the Retinex filter, which used a color restoration algorithm with contrast enhancement to contrast the spray droplets from the background. Next, the images were run through the BaSiC plugin, which corrected the varying illumination and background bleaching in the photoset from the x-ray light source. A median Z-Project and subtract command was used next to select and remove static imperfections in each photo, namely from particles resting on the camera lens. The photos were then used with a Noise2Void command from the CSB Deep plugin, which first created and trained a de-noising algorithm as a reference model to later remove background noise in each photo. After de-noising, the photos were thresholded and used in conjunction with the Trackmate plugin, which performed tracking, data visualization, and track analysis and output to a spreadsheet where the data could be used for droplet size distribution computation.

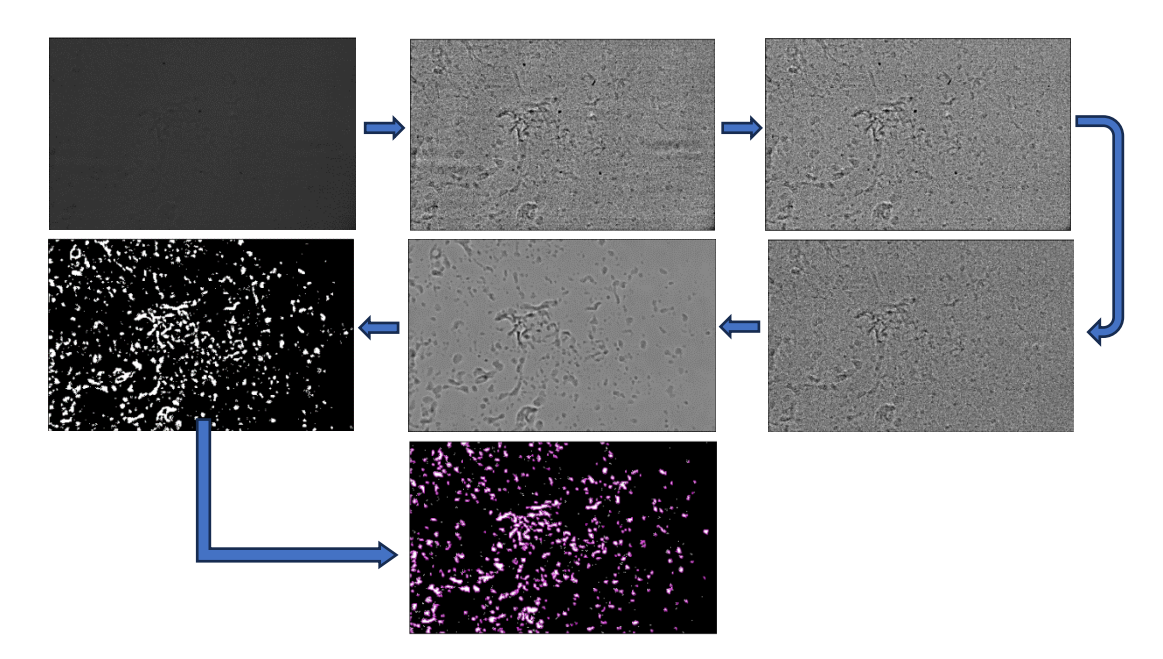


Fig. 4 Flowchart of image processing (from raw image to processed image; image dimension: 0.75 mm x 1.2 mm).

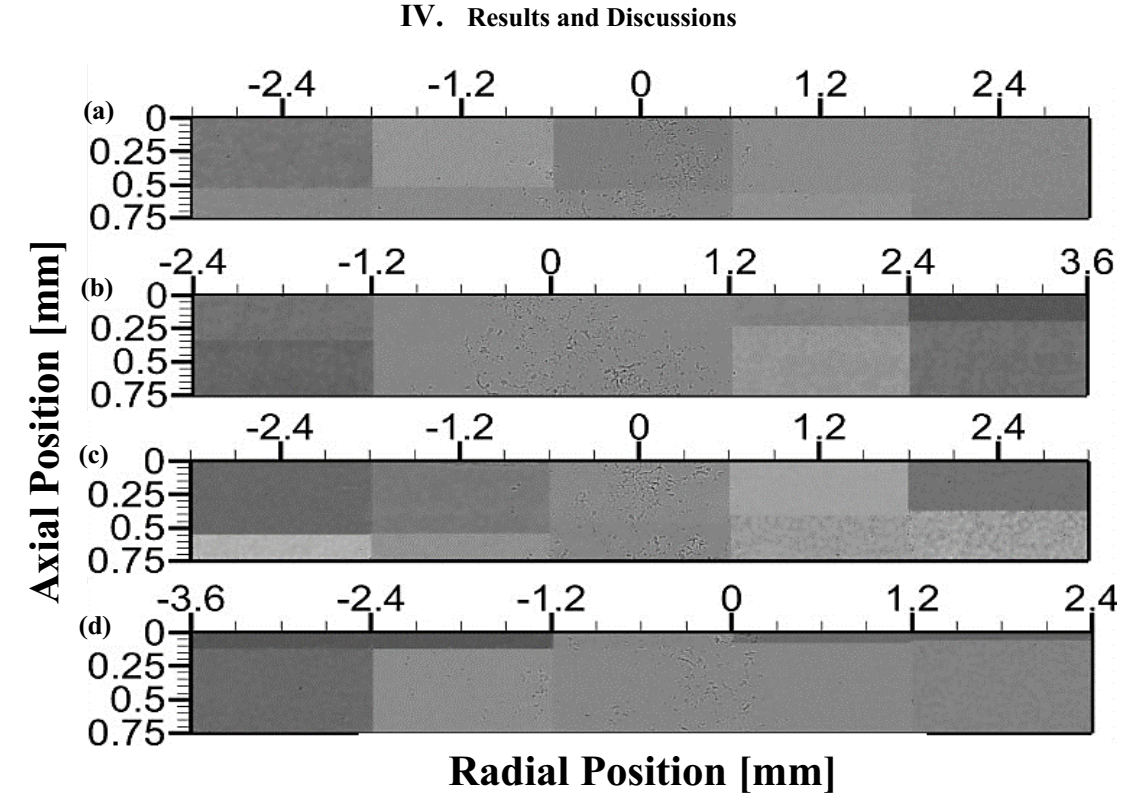


Fig. 5 Raw spray image near injector exit of (a) SBS, (b) SBP, (c) SBC and (d) SBCR Injector

Figure 5 shows sample processed combined images at the near injector exits for different SB sprays in the injector near field. X-ray images show varying darkness and lightness due to the interplay of two key factors: x-ray attenuation and x-ray decay. The first set of images for the axial planes of each injector right after the injector exits are

not consistent. Also, note along the flow direction, the first axial plane imaged for each FOV (1.2 mm x 0.75 mm) includes part of the injector body, the injector exit, and the external spray discharged from the exit. Due to the small axial dimension, 0.75 mm in length, the injector could not be monitored at the exact position for each injector, nor with the injector exit at the same axial location in the first FOV of 0.75 mm long. It might also happen due to slight tilting, displacement of injector body or camera positioning during the experimentation. Consequently, some injectors have smaller portions of image with sprays, and some have larger portions remaining for the first set of images by defining Y = 0 as the plane of the injector exit. That is, in the Fig. 5, for each injector, each image is combination of part of the originally  $1^{st}$  set of FOVs including the injector exit, and part of the neighboring downstream FOV. In the droplet size analysis in the later section, pointwise Sauter mean diameter (SMD) is quantified in each FOV (1.2 mm x 0.75 mm) based on the working principle of a pointwise phase doppler particle analyzer that measure the SMD of droplets passing a volume of beam diameter of  $\sim 0.5 - 2$  mm. Thus, in the later section, y in the figures is taken as the average of the upper and lower bound of each FOV (each measuring point for droplet sizing) with length of 0.75 mm is taken. As a result, the axial locations for these injectors are not also the same further downstream Y values as they are subsequent locations. The location difference is within the uncertainty of the displacement of the traversing-system-controlled optical table.

From Fig. 5, all the SB injectors generated fine droplets immediately. Qualitatively, the SBC injector seems to have yielded finer sprays. This might be because of (1) the higher shear layers at zones outside of the injector exit that enhanced secondary atomization; (2) additionally, the continuous direction from the primary to secondary swirls increases the vorticity of the AA, which might explain the enhanced atomization and finer droplets. Time-space analysis of near-field droplet size and size distribution in the later section gives insight into the spray characteristics and how it possibly relates to internal bubble formation and external bubble stability, which in turn reveals the best swirl placement for optimal experimental results.

Figure 6 illustrates the cumulative density profiles of droplet size at all the probed radial locations, each with 128 consecutive images, for different axial planes in the injector near field for all the four injectors. The MATLAB code is obtained based on the working principle of the point-wise Phase Doppler Particle Analyzer (PDPA) that calculates the SMD of droplets passing a small volume of a laser beam with a diameter of about ~0.5-2 mm. In the current study, each FOV represents one measurement location similar to the measuring point by the PDPA. As aforementioned, the axial planes differ for the injectors due to the slight different locations of the injector exit (Y = 0)in the first set images (0.75 mm long) that include the injector exit. At the axial plane of Y = 0.269 mm, around 90 percent of droplets have diameters under 17 µm for the SBS injector as demonstrated in Figure 6(a). Figure 6 also shows that the SBP, SBC, and SBCR injectors generate around 90 percent of the droplets with diameters less than 16  $\mu m$ , 18  $\mu m$  and 15  $\mu m$  at the axial planes immediate near to the injector exit respectively. Close to Y = 0.75 mm, SBS, SBP, SBC and SBCR injectors generate around 88%, 86%, 90% and 91% of the droplets under 18 µm, respectively. Close to Y = 3 mm, SBS and SBP injector perform better with 94% and 95% of the droplets under 18 µm respectively, where SBC and SBCR injector generate 86% and 88% of the droplets, respectively. This might be attributed to some droplet collision adjacent to the injector exit due to the combined external and internal swirling flows of the SBC and SBCR. Further downstream near to Y = 9 mm, SBS injector generates 98% of the droplets under 18  $\mu$ m, where SBP, SBC and SBCR injector produce 97%, 91%, 96% of the droplets, respectively. Regardless of the slight variations, the cumulative density profiles are almost identical for all the SB injectors, and more than 95% of droplets are under 18 um. The results from Figure 6 show that SBS, SBP, SBC and SBCR injectors generate comparably fine sprays immediately at the exit orifice and further downstream due to the enhanced primary and secondary atomization.

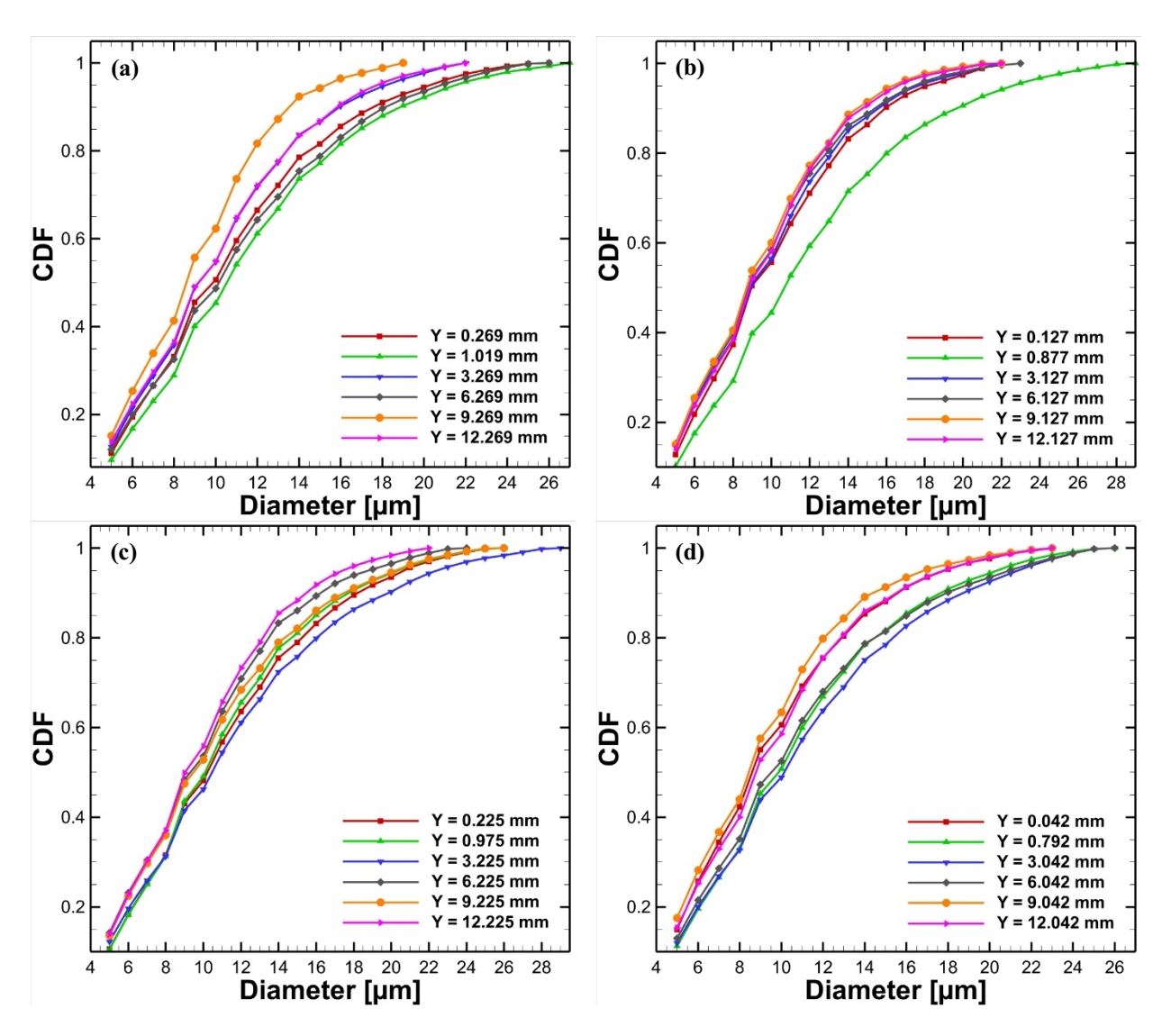


Fig. 6 Radial profiles of cumulative density function (CDF) of (a) SBS, (b) SBP, (c) SBC and (d) SBCR injectors at various axial planes.

Figure 7 shows the radial profile of SMD at different axial planes, denoted as Y, with X = 0 representing the spray center. The injector exit is denoted by Y = 0 mm. The SMDs are computed at each measured location (i.e., each FOA) for the entire set of consecutive 128 images captured one time. Figure 8 illustrates the SMD contours for the different SB injectors with the magnitude of SMD represented by the colors. From Fig. 8, the SBP injector generates wider spray than the other SB injectors, where the SBS injector shows the least wide spray among these injectors. Note that, Fig. 8 only qualitatively show the spray width trend due to the different x and y scales, and the limited number of images that can be captured by the ultra-fast x-ray imaging. In Fig. 7, the radial profiles of the SMD from SBP injector are computed from spray width of X = -10.8 mm to 9.6 mm from Fig. 8, beyond which no droplets observed during the experiments. The radial profiles of the SMD from SBS are computed from the radial span of X = -7.2 mm to 8.4 mm. The radial ranges for the SBC injector and SBCR injector are X = -9.6 mm to 7.2 mm and X = -7.8 mm to 9 mm, respectively. For all the SB injector configurations, the SMD is lower than 18 µm, indicating the immediate fineness due to the powerful SB atomization. At the injector exit, SBS and SBP in Fig. 7a-b forms comparable fine droplets with slight improvement in SBP. More specific, the SMD at the axial plane closer to injector exit is around 15  $\mu m$  at  $\sim X = 0$  mm for SBS injector; and  $\sim 14.5$   $\mu m$ , 18  $\mu m$  and 13  $\mu m$  for the SBP, SBC and SBCR injector, respectively. In Fig. 7d, SBCR forms the smallest SMD representing the combined effectiveness of internal and external swirl in the injector near field. In comparison, the SBC forms the largest SMD at the injector exit, which is possibly due to the droplet collision promoted by the external and internal swirling AA in the same direction. Even with the more apparent collision in the SBC, the SMD reduces along the axial direction, reflecting the ongoing secondary atomization, and ultimately achieves the comparable final SMD of  $\sim$ 12  $\mu m$  at Y =  $\sim$ 12 mm for all the SB injectors. The SBCR achieve this final SMD with more smooth transition with the peak SMD < 16  $\mu m$  in the injector near field, again indicating the effective primary and secondary atomization, and the corporate effect by the external and internal swirls at the reverse direction. Furthermore, the more uniform SMD radial profile in the injector near field signifies that the SBCR also generates droplets with more even size distribution. The slightly higher SMD values in the profiles observed for the SBS at axial locations Y = 3.269 mm are insignificant and it could occur due to the occasionally bigger sized droplets. Overall, the results show that the SBCR injector generates finer droplets within Y = 0.042 mm with rapid completion of atomization and uniform droplet size distribution, compared to other SB injectors. It also shows the further improved secondary atomization than other SB injectors.

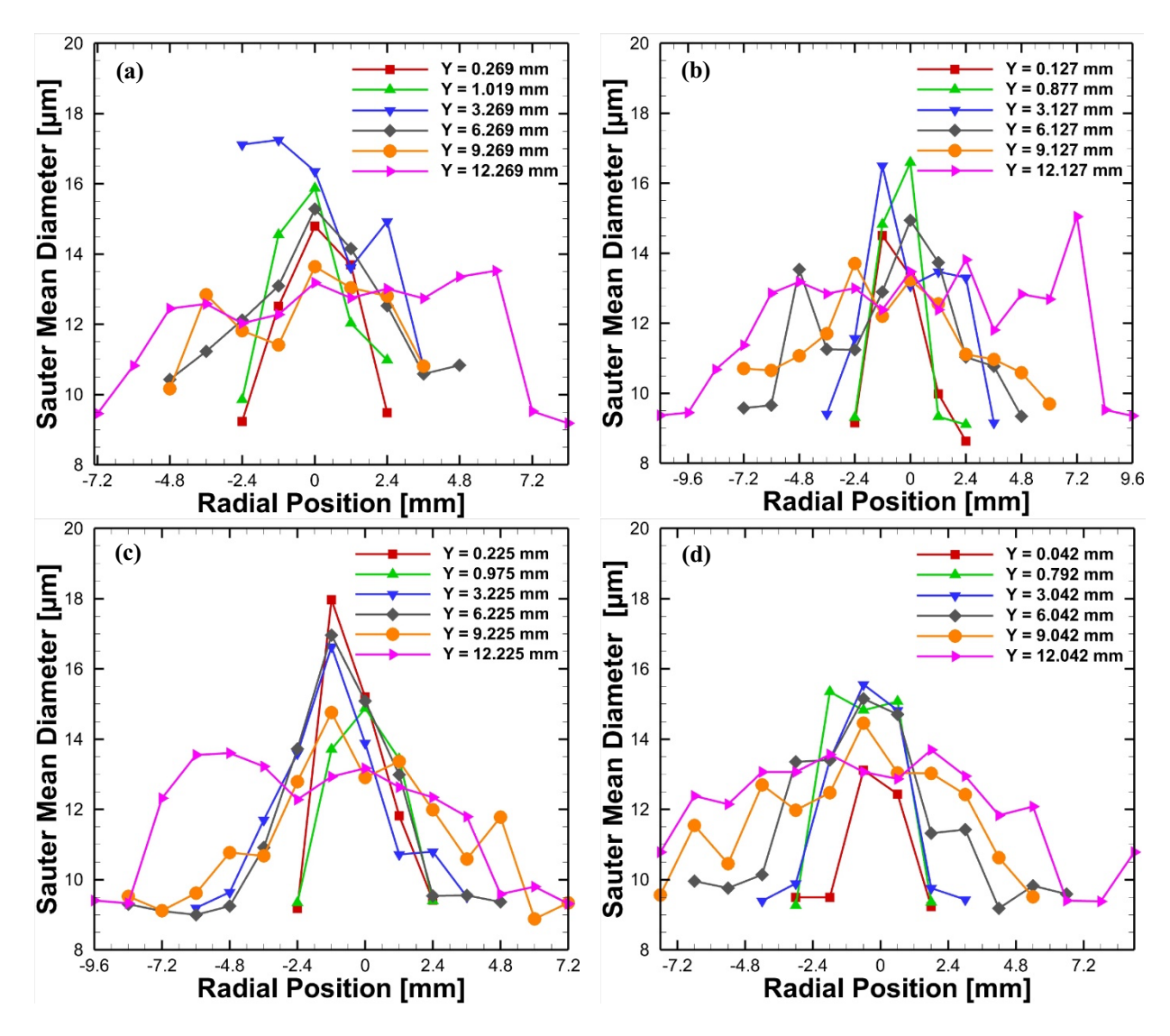


Fig. 7 Radial profiles of SMD of (a) SBS, (b) SBP, (c) SBC and (d) SBCR injectors at various axial planes.

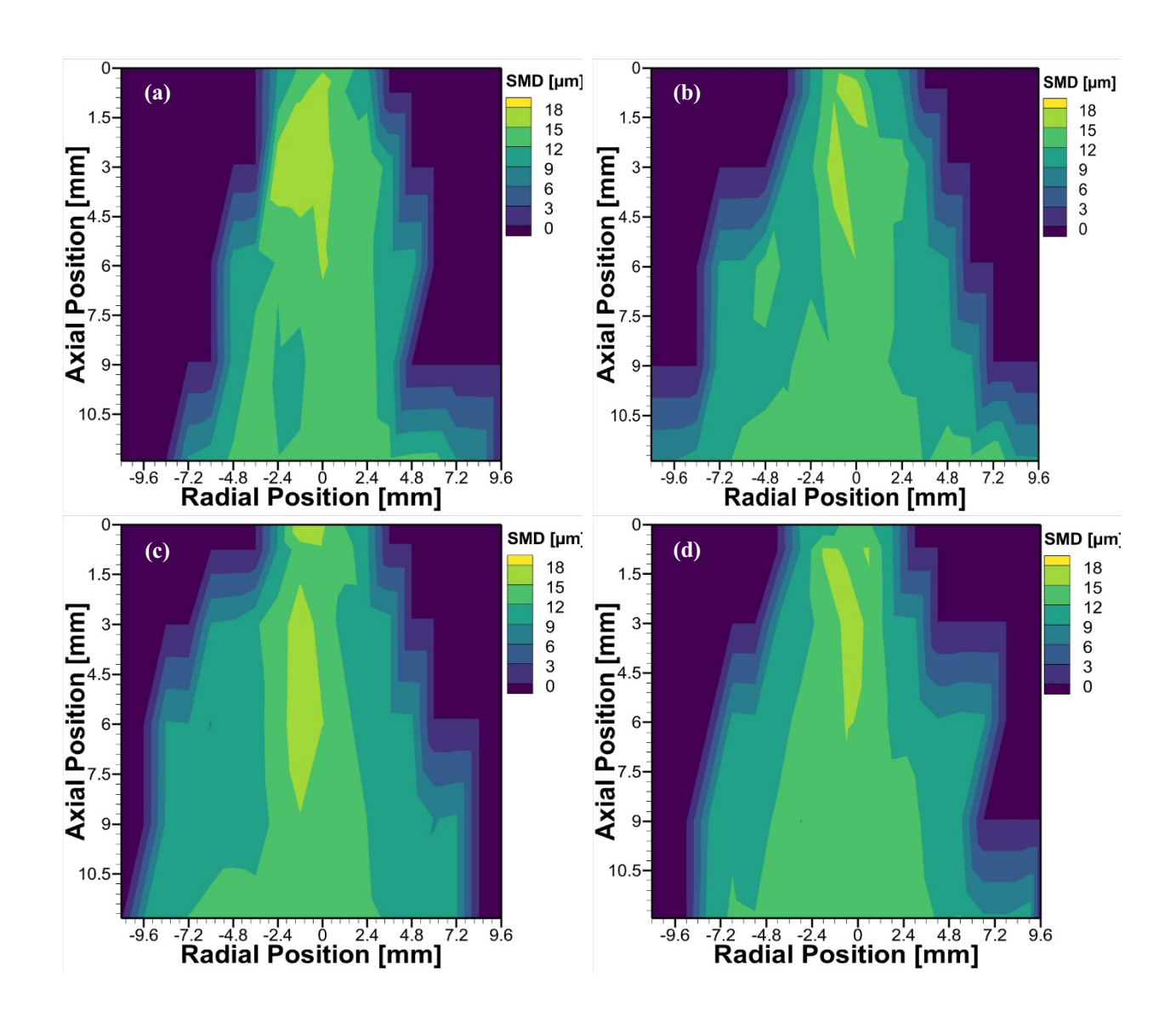


Fig. 8 SMD Contours of (a) SBS, (b) SBP, (c) SBC and (d) SBCR injectors in the injector near field.

Figure 9 shows the temporal evolution of SMD at the selected locations. Different axial planes are selected to compare the fluctuations of SMD values along the axial direction to gain insight into secondary atomization disintegrating droplets and the spray stability with the induced swirling flows internally and/or externally. Three axial planes are chosen to analyze the completion of secondary atomization with three different radial positions such as spray center, periphery of the spray and in between the spray center and periphery for those axial planes. At the injector exit, SBP and SBC show superior stability reflected by the less fluctuation of SMD with time, with SBS shows the largest fluctuation. At further downstream, Y > 6 mm, SBCR showed the slight fluctuation with respect to time, indicting the high stability regardless of the fluctuation at the injector exit. Despite the variations with the injector near region, temporally uniform SMD is observed at the further downstream,  $Y = \sim 9$  mm, for all the SB injectors, indicating the stability of the SB concept with the external and/or internal swirls.

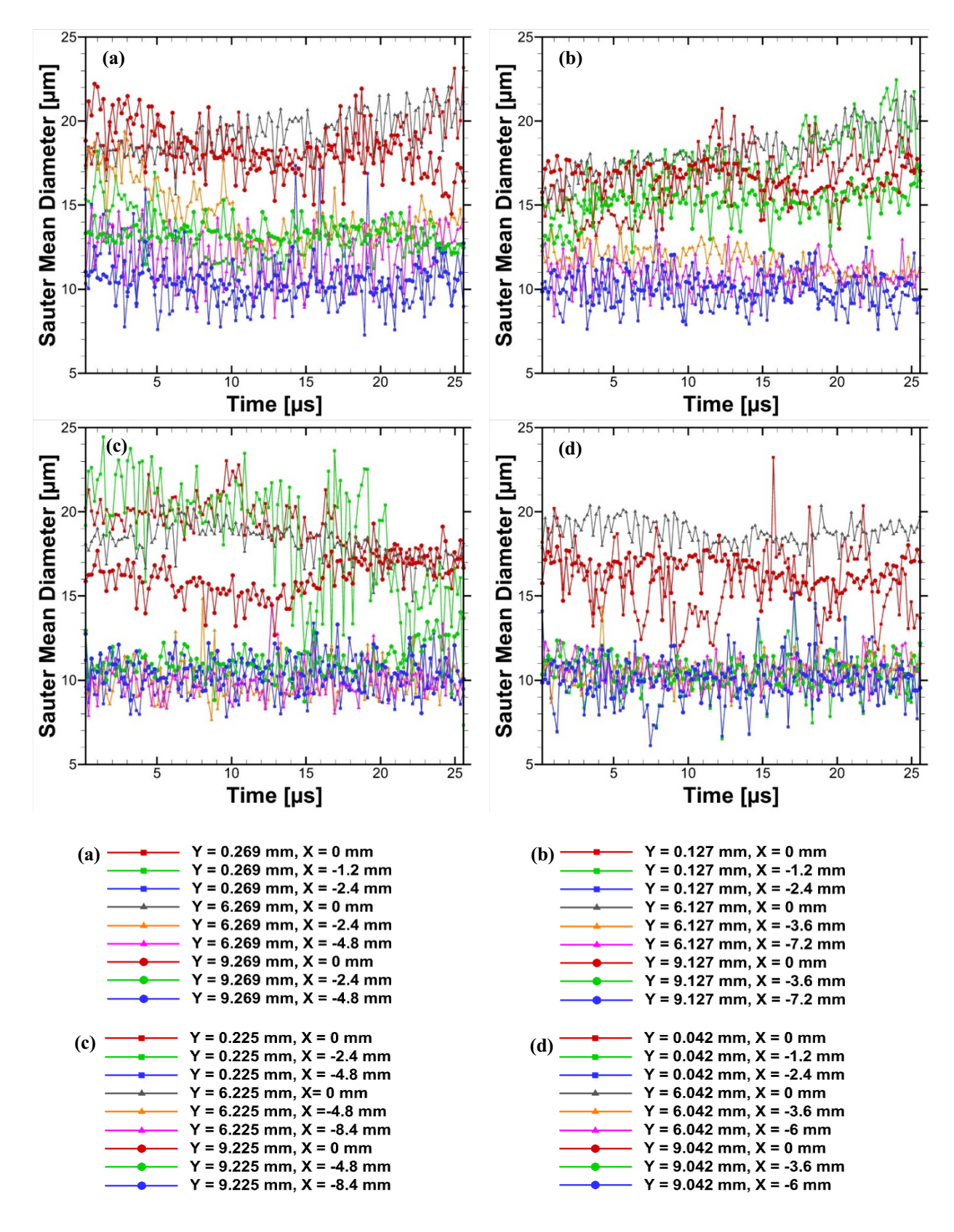


Fig. 9 SMD as function of time for (a) SBS, (b) SBP, (c) SBC and (d) SBCR injectors at selected locations.

Figure 10 indicates an example of uncertainty analysis of the droplet sizing process. The current droplet sizing is based on how the boundary of each droplet is detected by differentiating the gray scale with the surrounding. If the object has a different average gray level from that of its surrounding, the effect of thresholding will produce a white object with a black background or vice versa, affecting the droplet boundary detection and thus affecting the droplet detection and the consequent sizing. In Figure 10, an image is analyzed (Y = 0.75 mm, X = 0 mm from SBP injector) as example. Threshold dialog allows to identify pixels above a threshold, below a threshold, or falling between two thresholds. Threshold value is calculated using the formula below in Eqn 2. From Fig. 10, only 6.1% of all the particles are identified because the thresholding limit is set between -17.69 and - $\propto$ . If the thresholding limit changes, the number of detected particles will also change accordingly. If the number of detected particles changes, it will affect the overall analysis. For the analysis, the auto-thresholding was used. But the fact is that the threshold limit data is very fluctuating and not consistent. That is why one example is given to show the fact. The future work will develop the approach to further analyze the threshold limits of each of the frames, if possible, and estimate the uncertainty of the droplet sizing process based on this example.

$$threshold = \frac{average\ background\ + average\ objects}{2} \tag{2}$$

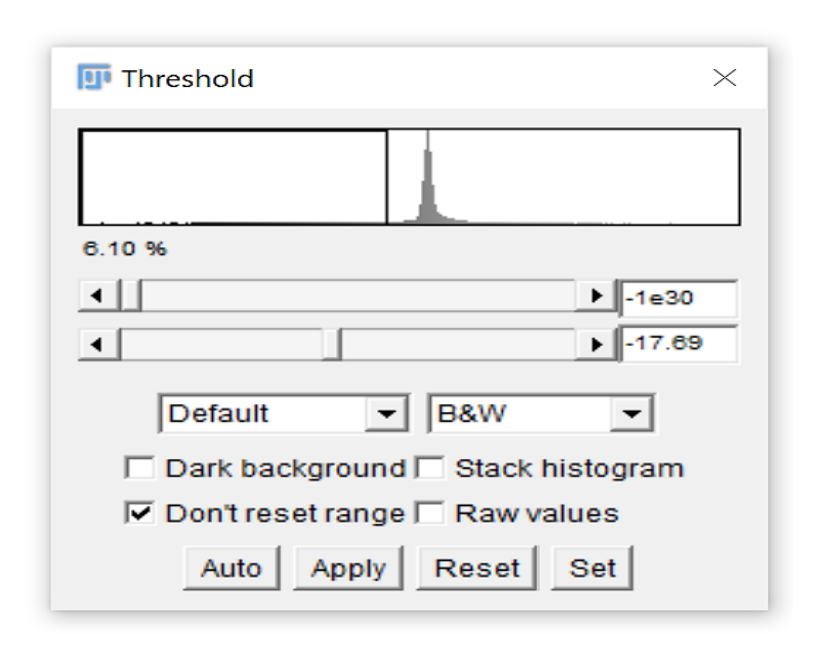


Fig.10 Thresholding of images using ImageJ software.

## V. Conclusion

The results show that all the SB injectors consistently produce finer droplets immediately at the exit orifice and further downstream. The cumulative density profiles are similar for all the SB injectors where more than 95% of droplets are under 18  $\mu$ m. The radial profile analysis of SMD has revealed that the SBCR injector generates more uniform spray with overall finer sprays immediately compared to the other SB injectors, indicating the effective reverse external and internal swirls for enhanced primary and secondary atomization. SBP injectors shows the widest sprays among the other three injectors, where SBS injector generates the least wide spray. SBC and SBCR injectors show

similar spray width, but wider than that of SBS, benefiting fuel dispersion in a gas turbine engine. SBC and SBP shows stability at the injector exit superior to that of SBS and SBCR. Regardless, SBCR results in high stability at further downstream, Y > 6 mm, with stability achieved at Y = 9 mm for all the SB injectors. In summary, all the SB injectors have produced comparable finer droplets. The SBCR injector has showed the most uniform SMD values, i.e., uniform sprays and improved stability of sprays compared to the other SB injectors. Future work will use the time-resolved laser-driven shadowgraph imaging to quantify the entire spray at one time (vs each small FOV allowed by the X-ray imaging) in the injector near field to quantitatively estimate the spray characteristics (e.g., angles, atomization completion length) and the spray stability.

#### Acknowledgements

The current research is funded by the Startup fund of Baylor University and NSF CIVIC award No. 2228311 and No. 2322319. This work is being conducted at Advanced Photon Source (APS) beamline 32-ID at Argonne National Lab based on the awarded beamtime under the GUP #80526. We would like to thank Mrs. Rachel Swinney to assist with data collection, and Mr. Alex L. Deriy, the Beamline Instrumentation Specialist, who helped facilitate the easy and efficient experimental setup. We also sincerely appreciate Mr. Presley Mogote, Mr. John Cary, Mrs. Karly Jackson, and Mr. Curtis Jackson's assistance on injector SolidWorks design, manufacturing, and/or experimental setup.

#### References

- [1] Jiang, L., Agrawal, A. K., and Taylor, R. P., "Clean Combustion of Different Liquid Fuels Using a Novel Injector," *Experimental Thermal and Fluid Science*, Vol. 57, 2014, pp. 275–284. https://doi.org/10.1016/j.expthermflusci.2014.05.002
- [2] Jiang, L., and Agrawal, A. K., "Investigation of Glycerol Atomization in the Near-Field of a Flow-Blurring Injector Using Time-Resolved PIV and High-Speed Visualization," *Flow, Turbulence and Combustion*, Vol. 94, No. 2, 2015, pp. 323–338. https://doi.org/10.1007/s10494-014-9572-2
- [3] Jiang, L., and Agrawal, A. K., "Spray Features in the near Field of a Flow-Blurring Injector Investigated by High-Speed Visualization and Time-Resolved PIV," *Experiments in Fluids*, Vol. 56, No. 5, 2015, p. 103. https://doi.org/10.1007/s00348-015-1973-z
- [4] Qavi, I., and Jiang, L., "Optical Characterization of Near-Field Sprays for Various Alternative and Conventional Jet Fuels Using a Flow-Blurring Injector," *Flow, Turbulence and Combustion*, Vol. 108, No. 2, 2022, pp. 599–624. https://doi.org/10.1007/s10494-021-00276-9
- [5] Qavi, I., Jiang, L., and Akinyemi, O. S., "Near-Field Spray Characterization of a High-Viscosity Alternative Jet Fuel Blend C-3 Using a Flow Blurring Injector," *Fuel*, Vol. 293, 2021, p. 120350. https://doi.org/10.1016/j.fuel.2021.120350
- [6] Gañán-Calvo, A. M., "Enhanced Liquid Atomization: From Flow-Focusing to Flow-Blurring," *Applied Physics Letters*, Vol. 86, No. 21, 2005, p. 214101. https://doi.org/10.1063/1.1931057
- [7] Jiang, L., and Agrawal, A. K., "Combustion of Straight Glycerol with/without Methane Using a Fuel-Flexible, Low-Emissions Burner," *Fuel*, Vol. 136, 2014, pp. 177–184. https://doi.org/10.1016/j.fuel.2014.07.027
- [8] Simmons, B. M., and Agrawal, A. K., "Flow Blurring Atomization for Low-Emission Combustion of Liquid Biofuels," *Combustion Science and Technology*, Vol. 184, No. 5, 2012, pp. 660–675. https://doi.org/10.1080/00102202.2012.660222
- [9] Danh, V., Akinyemi, O. S., Taylor, C. E., Frank, J. T., and Jiang, L., "Effect of Injector Swirl Number on Near-Field Spray Characteristics of a Novel Twin-Fluid Injector," *Experiments in Fluids*, Vol. 60, No. 5, 2019, p. 80. https://doi.org/10.1007/s00348-019-2721-6
- [10] Danh, V., Jiang, L., and Akinyemi, O. S., "Investigation of Water Spray Characteristics in the near Field of a Novel Swirl Burst Injector," *Experimental Thermal and Fluid Science*, Vol. 102, 2019, pp. 376–386. https://doi.org/10.1016/j.expthermflusci.2018.12.014
- [11] Akinyemi, O. S., and Jiang, L., "Development and Combustion Characterization of a Novel Twin-Fluid Fuel Injector in a Swirl-Stabilized Gas Turbine Burner Operating on Straight Vegetable Oil," *Experimental Thermal and Fluid Science*, Vol. 102, 2019, pp. 279–290. https://doi.org/10.1016/j.expthermflusci.2018.11.014
- [12] Akinyemi, O. S., Jiang, L., Hernandez, R., McIntyre, C., and Holmes, W., "Combustion of Straight Algae Oil in a Swirl-Stabilized Burner Using a Novel Twin-Fluid Injector," *Fuel*, Vol. 241, 2019, pp. 176–187. https://doi.org/10.1016/j.fuel.2018.12.006
- [13] Khandelwal, B., Lili, D., and Sethi, V., "Design and Study on Performance of Axial Swirler for Annular Combustor by Changing Different Design Parameters," *Journal of the Energy Institute*, Vol. 87, No. 4, 2014, pp. 372–382. https://doi.org/10.1016/j.joei.2014.03.022

[14] Faeth, G. M., "Swirl Flows: A. K. Gupta, D. G. Lilley, and N. Syred, Abacus Press, Tunbridge Wells, England, 1984, Xiii + 475 Pp, \$50.00," *Combustion and Flame*, Vol. 63, No. 1, 1986, p. 311. https://doi.org/10.1016/0010-2180(86)90133-1

.